

# Physical Parameters and Chemical Composition of a Nitrogen DC Discharge with Water Cathode

Sergey A. Smirnov<sup>1</sup> · Dmitriy A. Shutov<sup>1</sup> ·  
Elena S. Bobkova<sup>2</sup> · Vladimir V. Rybkin<sup>1</sup>

Received: 13 February 2015 / Accepted: 26 March 2015 / Published online: 8 April 2015  
© Springer Science+Business Media New York 2015

**Abstract** This paper reports the results of the experimental study and chemical composition modeling for a DC nitrogen discharge burning above water cathode in the pressure range of 0.1–1 bar and at discharge current of 40 mA. The gas temperature, vibrational temperatures, reduced electric field strength, cathode voltage drop, and emission intensities of some nitrogen bands were obtained from experiment. The modeling chemical composition of plasma was carried out on the basis of these data. At modeling, the combined solution of Boltzmann equation for electrons, equations of vibrational kinetics for ground states of N<sub>2</sub>, O<sub>2</sub>, H<sub>2</sub>O and NO molecules, equations of chemical kinetics and plasma conductivity equation were used. The calculations agree with the measured bands intensities for the second positive system of N<sub>2</sub> and vibrational temperatures of N<sub>2</sub>(C<sup>3</sup>Π<sub>u</sub>). In the frame of the model proposed, the data of other studies were explained. The second kind collision of electrons with N<sub>2</sub> vibration excited states was shown to affect strongly the electron gas parameters. The electron average energy and electron density are given. The difference between the properties of the discharges in N<sub>2</sub> and air at the same conditions are discussed as well.

**Keywords** DC nitrogen discharge · Water cathode · Modeling · Plasma composition · Electron parameters

## Introduction

In recent years the interest in non-thermal plasmas in contact with liquids has increased significantly [1]. This is mainly due to their ability to form strongly chemically active species (OH, O, H<sub>2</sub>O<sub>2</sub>, nitrogen oxides etc.), UV radiation and shock waves. As a result,

---

✉ Vladimir V. Rybkin  
rybkin@isuct.ru

<sup>1</sup> Department of Microelectronic Devices and Materials, Ivanovo State University of Chemistry and Technology, Ivanovo, Russia

<sup>2</sup> Department of Industrial Ecology, Ivanovo State University of Chemistry and Technology, Sheremetev Ave., 7, Ivanovo 153000, Russia

plasmas in contact with liquids are very effective for carrying out many oxidative and reducing processes in a liquid phase. Among these processes it is possible to point out the numerous environmental applications [2, 3].

For estimation of possibilities of discharge action, it is necessary to know the active species concentrations in a gas phase and their change under alterations of discharge parameters. Such data are rather limited. The emission spectra show usually the radiation bands of excited states of  $N_2$ , OH and NO and lines of atomic H and O at discharge in nitrogen containing gases [4–6]. As far as the discharges in contact with water are concerned, there are some studies where the OH radical concentrations in the ground state were measured in a gas phase for the atmospheric pressure DC discharge in an ambient air, He, Ar and  $N_2$  by a LIF method [6, 7] and applying the absorption in UV region for Ar/ $H_2O$  [8]. For nitrogen, it was discovered that OH concentration was about  $(2\text{--}2.3) \times 10^{15} \text{ cm}^{-3}$  in the current range of 15–30 mA. It is safe to say that measurements of species densities in liquid plasmas are largely an unexplored area. For this reason, modeling becomes an efficient method to study plasma composition. For these reasons, the large number of works devoted to plasma chemistry modeling was published in recent years.

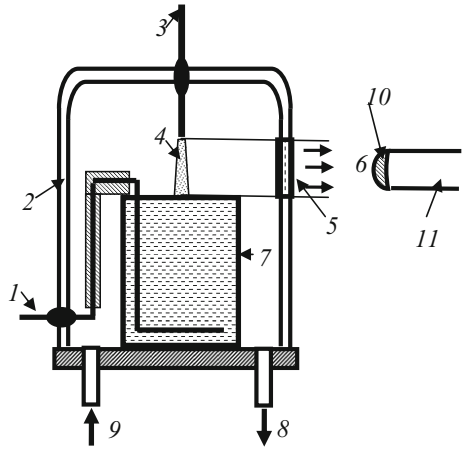
Thus, in study [9], a zero-dimension Global model was proposed for the helium RF atmospheric pressure discharge with admixture of water molecules. In study [8], a zero-dimension modeling of the chemical composition was accomplished for an atmospheric pressure argon plasma jet flowing into humid air. The reaction chemistry included 84 different species and 1880 reactions. Modeling results agreed satisfactorily with ozone concentrations measured in study [10] by adsorption method. Simulation of the NO and O formation-loss mechanism in the RF atmospheric pressure needle-type plasma jet (Ar + 2 % of air) was carried out in study [11]. For the model verification, the concentrations of NO molecules and O atoms, measured experimentally were used. The simulation of plasma chemical reactions was carried out in study [12] for argon DC discharge above water cathode in the pressure range of (0.1–1) bar. Calculated line intensities of Ar atom emission agree well with experimental ones. All models mentioned above did not consider the kinetics of vibrational states. Probably, for plasmas containing noble gases presumably it is not too important. But the modeling of atmospheric pressure DC discharge in air [13] and experimental data [14, 15] showed that effective vibrational temperatures ( $\sim 5000$  K) of  $N_2$  are essentially more than translation ones ( $\sim 1500$  K). Therefore, vibrationally excited molecules (VEM) can influence strongly the electron energy function distribution (EEDF) over super elastic collisions.

As far as we know, there is no detailed analysis of kinetics of the processes taking place in a nitrogen DC discharge burning above the water cathode. The main aim of the given work is to develop the model allowing describing the plasma composition. The model proposed will take into consideration the influence of chemical composition and VEM on EEDF and vice versa. For the model checking the emission intensities of nitrogen bands and vibrational temperatures of  $N_2(C^3\Pi_u)$  state will be used.

## Experimental

Figure 1 represents a principal scheme of the experimental set-up. The glass cell with distilled water of 80 ml volume was placed into a 5 l glass vacuum-tight bell-jar. Molecular nitrogen of the ultra high purity grade was applied as a plasma-forming gas. The gas flow rate was  $300 \text{ cm}^3/\text{s}$ . At lower gas flow rate, the formation of condensed water was

**Fig. 1** Schematic diagram of the experimental set-up. 1 cathode, 2 glass bell-jar, 3 anode, 4 discharge, 5 quartz window, 6 radiation output to entrance lens of light fiber, 7 glass cell with distilled water, 8, 9 gas outlet and inlet, 10 entrance lens of light fiber, 11 light fiber



observed and we could not measure correctly the emission intensities. The anode was made from mechanically sharpened stainless steel wire. A high voltage (up to 4 kV) was applied between the aqueous cathode and anode, which was placed at the position 1–10 mm (typically 10 mm) above the water surface. The distance between the anode and the liquid surface was adjustable. The discharge current was 40 mA. The N<sub>2</sub> pressure was varied from 0.1 to 1(±0.01) bar. For the emission spectra digital registration the AvaSpec-2048FT-2 monochromator (grating of 600 line/mm) was used. The light entered the monochromator entrance slit through a quartz optical fiber. The light guide-monochromator system was calibrated by the monochromator manufacturer on a radiation power. The emission from cathode and anode discharge parts was cut off by the size of the quartz window.

The average on the discharge volume bands intensity,  $\bar{I}$ , was determined as follows. The quanta amount,  $d\Phi$ , emitted with the discharge volume  $dV$  into solid angle  $\Omega(r, \varphi, z)$  per unit of time is

$$d\Phi = \frac{I}{4 \times \pi} \times \Omega \times dV = \frac{I(r, \varphi, z)}{4 \times \pi} \times \Omega \times r dr d\varphi dz,$$

where  $I$ —the integral band intensity [quantum/(s × cm<sup>3</sup>)];  $r, \varphi$  and  $z$ —cylindrical coordinates of emitting discharge point. Since the discharge radius ( $R_D \approx 1$  mm) and discharge length ( $L_D = 10$  mm) are much less than the distance between the light guide entrance lens and the discharge ( $L = 75$  mm), the  $\Omega$  value is approximately the same for every discharge point and equals to

$$\Omega = \frac{\pi \times R_L^2}{L^2},$$

where  $R_L$ —radius of entrance lens (2.5 mm).

Therefore, the total amount of quanta,  $\Phi$ , which is registered by monochromator per second, can be written as

$$\Phi = \frac{R_L^2}{4 \times L^2} \times \int_0^{R_D} \int_0^{2\pi} \int_0^{L_D} I \times r dr d\varphi dz = \frac{R_L^2}{4 \times L^2} \times \bar{I} \times V_D,$$

where  $\bar{I}$ —average on the discharge volume intensity,  $V_D$ —discharge volume.

For the determination of the electric field strength,  $E$ , and the cathode voltage drop,  $U_c$ , the voltage drop between anode and cathode was measured as a function of anode-surface water distance. The digital voltmeter Fluke 289 © (USA) was used for this purpose. Voltage drop on water layer was measured at a contact of anode with water surface. Then, this value was subtracted from the total voltage measured. The linear part of volt-distance dependence was treated with a least-squares method to obtain the electric field strength in a plasma column. The extrapolation of dependence to a zero distance gives the  $U_c$  value. This value is partly overestimated since we did not take into account the anode voltage drop. But it is well known that the anode voltage drop is essentially less than cathode one [16].

The rotational temperature was determined from non-resolved rotational structure of the band for the  $C^3\Pi_u \rightarrow B^3\Pi_g$  (0–2) transition as it was described elsewhere [4]. In the present case, the rotational temperature is equal to the translational one. The MDR-23 spectrometer was utilized for checking possibility of this method. Its resolution (grating of 1200 line/mm) allowed to obtain the resolved structure of  $R_1$ -branch (for  $J' > 15$ ) and unresolved one depending on the split sizes. The temperatures difference obtained with both methods was not more than 40 K.

The reproducibility errors for all measured values were calculated on the base of five and more measurements using the confidence probability of 0.95. The total errors are shown in appropriate Figures as the bars.

All measurements were carried out after reaching the stationary conditions. It was controlled by temporal behavior of line intensities (actually, in 15 min of discharge burning).

## Description of the Model and Calculations

The model was described with the Boltzmann equation for electrons, chemical kinetics equations, equations of vibration kinetics, and the equation of plasma conductivity. The last one was used for the determination of electron density on the base of the measured current density.

The EEDF was obtained as the solution of the homogeneous Boltzmann equation using the two-term expansion. Collision integrals include the collisions of electrons with  $H_2$ ,  $N_2$ ,  $O_2$ ,  $H_2O$ ,  $NO$  molecules in electronic ground state and with  $O(^3P)$  atoms. The collisions of the second kind with vibrationally excited molecules and e–e collisions were taken into consideration as well. The cross-section sets for  $N_2$ ,  $O_2$ ,  $H_2O$ ,  $NO$ ,  $H_2$  molecules and  $O(^3P)$  atoms were taken from studies [17–22], respectively. Some details of the solution were described by us elsewhere [15, 23].

The Boltzmann equation was written as

$$\frac{d}{d\varepsilon} \left( \beta \frac{df}{d\varepsilon} \right) = J_e + J_{ine} + J_{ee}, \quad (1)$$

where  $\varepsilon$ —in the electron energy,  $f(\varepsilon)$  is EEDF with the following normalization

$$\int_0^{\infty} f(\varepsilon) \varepsilon^{1/2} d\varepsilon = 1.$$

In Eq. (1),  $\beta$  is expressed in S.I. units by:

$$\beta = \frac{e^2}{3} \left(\frac{E}{N}\right)^2 \times \left(\sum_i \sigma_i^{tr} Y_i\right)^{-1} \times \varepsilon, \tag{2}$$

where  $E/N$ ,  $e$  are the reduced electric field strength and the electron charge, respectively,  $\sigma_i^{tr}$  is the momentum transfer cross-section for electron collisions with heavy particles  $i$ ,  $Y_i$  is mole fraction of this type of particle.

$J_e$  is given by:

$$J_e = -\frac{d}{d\varepsilon} \left(kT \times \gamma \frac{df}{d\varepsilon} + \gamma \times f\right), \tag{3}$$

where  $T$  is the gas temperature, and,

$$\gamma = 2m_e \times \left(\sum_i \frac{\sigma_i^{tr} \times Y_i}{M_i}\right) \times \varepsilon^2 + 6\varepsilon \times \sum_i hc \times (B_i \times \sigma_i^r \times Y_i),$$

where  $M_i$ ,  $B_i$ , and  $\sigma_i^{tr}$  are the mass, rotational constant ( $\text{cm}^{-1}$ ) and rotational excitation cross-section for heavy particles  $i$ .

The integral of inelastic collisions,  $J_{ines}$ , consists of two integrals,  $J_{un}^I$  and  $J_{un}^{II}$ , describing the collisions of the first and second kind, respectively:

$$J_{un}^I = \sum_i \sum_j Y_i \left[\varepsilon \cdot Q_j^I(\varepsilon) \cdot f(\varepsilon) - (\varepsilon + \varepsilon_{ji}) \cdot Q_j^I(\varepsilon + \varepsilon_{ji}) \cdot f(\varepsilon + \varepsilon_{ji})\right]$$

$$J_{un}^{II} = \sum_i \sum_j Y_i \left[\varepsilon \cdot Q_{-j}^I(\varepsilon) \cdot f(\varepsilon) - (\varepsilon - \varepsilon_{ji}) \cdot Q_{-j}^I(\varepsilon - \varepsilon_{ji}) \cdot f(\varepsilon - \varepsilon_{ji})\right]$$

where the summation is carried out on all  $j$  collisions for heavy particle  $i$ ;  $\varepsilon_{ji}$  is the threshold energy of process  $j$ ;  $Q_j^I$  is the cross-section of collision of the first kind and  $Q_{-j}^I$  is the cross-section of collision of the second kind. The relation between  $Q_j^I$  and  $Q_{-j}^I$  is given by the detailed balance principle:

$$Q_{-j}^I = \frac{\varepsilon - \varepsilon_{ji}}{\varepsilon} Q_j^I(\varepsilon + \varepsilon_{ji}).$$

The integral of e–e collisions,  $J_{ee}$ , has the form:

$$J_{ee} = -\frac{1}{8\pi} \left(\frac{e^2}{\varepsilon_0}\right)^2 \times Y_e \times \ln(\lambda) \times \frac{d}{d\varepsilon} \left[ f(\varepsilon) \int_0^\varepsilon \varepsilon^{1/2} f(\varepsilon) d\varepsilon + \frac{2}{3} \frac{df}{d\varepsilon} \left( \int_0^\varepsilon \varepsilon^{3/2} f(\varepsilon) d\varepsilon + \varepsilon^{3/2} \int_\varepsilon^\infty f(\varepsilon) d\varepsilon \right) \right], \tag{4}$$

where  $\varepsilon_0 = 8.854 \times 10^{-12} \text{ F} \times \text{m}^{-1}$  is the electric field constant and  $Y_e$  is the electron mole fraction.  $\ln(\lambda)$  is the Coulomb logarithm expressed by:

$$\ln(\lambda) = \ln \frac{(4\pi\varepsilon_0)^{3/2} (kT)^{1/2} \bar{\varepsilon}}{n_e^{1/2} e^3},$$

where  $\bar{\varepsilon}$  is the average electron energy and  $n_e$ —the electron concentration.

The Eq. (1) was solved by the following way. Let us take the uniform grid with the mesh point of 1.2...m...N. Integrating (1) on the one interval from  $\varepsilon_m$  to  $\varepsilon_{m+1}$

( $\Delta\varepsilon = \varepsilon_{m+l} - \varepsilon_m$ ) and calculating integrals of inelastic collisions using the method of rectangular trapeziums we obtain the system of  $(N - 2)$  difference equations:

$$a_m \cdot f_{m-1} - b_m \cdot f_m + c_m \cdot f_{m+1} = d_m. \tag{5}$$

The coefficients of this system are:

$$a_m = \left( \beta + \frac{kT}{e} \cdot \gamma \right)_m + \frac{1}{8\pi} \left( \frac{e^2}{\varepsilon_0} \right)^2 Y_e \cdot \ln \lambda \cdot \left[ \frac{2}{3} \frac{1}{\Delta\varepsilon} \left( \int_1^{\varepsilon_m} \varepsilon^{3/2} f d\varepsilon + \varepsilon^{3/2} \cdot \int_{\varepsilon_m}^{\varepsilon_N} f d\varepsilon \right) \right],$$

$$b_m = a_m + a_{m+1} + \gamma_m + \frac{\Delta\varepsilon}{2} \cdot \varepsilon_m \cdot \left( \sum_i \sum_j Y_i \cdot Q_{j,m}^i + \sum_i \sum_j Y_i \cdot Q_{-j,m}^i \right) + \frac{1}{8\pi} \left( \frac{e^2}{\varepsilon_0} \right)^2 \cdot Y_e \ln \lambda \int_{\varepsilon_1}^{\varepsilon_m} \varepsilon^{1/2} f_e d\varepsilon,$$

$$c_m = a_m + \gamma_{m+1} - \frac{\Delta\varepsilon}{2} \varepsilon_{m+1} \left( \sum_i \sum_j Y_i \cdot Q_{j,m+1}^i + \sum_j \sum_i Y_i \cdot Q_{-j,m+1}^i \right) + \frac{1}{8\pi} \left( \frac{e^2}{\varepsilon_0} \right)^2 \cdot Y_e \cdot \ln \lambda \cdot \left[ \frac{2}{3} \frac{1}{\Delta\varepsilon} \cdot \left( \int_{\varepsilon_1}^{\varepsilon_{m+1}} \varepsilon^{3/2} \cdot f d\varepsilon + \varepsilon_{m+1}^{3/2} \cdot \int_{\varepsilon_{m+1}}^{\varepsilon_N} f d\varepsilon \right) \right],$$

$$d_m = -\frac{\Delta\varepsilon}{2} \left[ \sum_i \sum_j Y_k \left( \varepsilon_{m+n_j+1} \cdot f_{m+n_j+1} \cdot Q_{j,m+n_j+1}^i + \varepsilon_{m+n_j} \cdot f_{m+n_j} \cdot Q_{j,m+n_j}^i \right) + \sum_i \sum_j Y_k \left( \varepsilon_{m-n_j+1} \cdot f_{m-n_j+1} \cdot Q_{-j,m-n_j+1}^i + \varepsilon_{m-n_j} \cdot f_{m-n_j} \cdot Q_{-j,m-n_j}^i \right) \right].$$

In these expressions the  $m, m + 1, m + 1 \pm n_j, m \pm n_j$  indexes correspond to number of grid point where appropriate value is determined. And  $\Delta\varepsilon = \varepsilon_{m+1} - \varepsilon_m, n_j = (\varepsilon_{ij} - \varepsilon_i) / \Delta\varepsilon + 1$ .

The boundary conditions for system (6) are

$$a_2 \cdot f_1 - (a_2 + \gamma_2) \cdot f_2 = 0, \tag{6}$$

$$(a_N + \gamma_N) \cdot f_N - a_N \cdot f_{N-1} = 0. \tag{7}$$

The summation of all Eqs. (5–7) gives zero. Therefore, the system developed is conservative one. That is it satisfies the condition of conservation of electron amount. Due to e–e collisions the system is not linear and equation members with inelastic collisions result in the matrix sparseness (existence of large amount of zero value). For this reason the application of standard procedures for the solution requires a large volume of calculation and computer memory. To avoid this the method of iterations combined with the sweep method was used. As the zero-order approximation the maxwellian EEDF with the average energy of 1 eV was used. Using this function the coefficients a, b, c, and d of (5–7) were calculated. This procedure transformed the equation system to formally three-diagonal form with the diagonal prevalence that provided the absolute stability of solution. After that the system was fast solved with a sweep method. The EEDF obtained was used as the next approximation. The calculation was terminated when the relative error was less than 0.0001.

The electron average energy, the reduced diffusion coefficient,  $D_e N$ , the electron drift velocity,  $V_D$ , and rate coefficients,  $K_{kj}$ , for electron impact were calculated using obtained EEDF:

$$\bar{\varepsilon} = \int_0^\infty \varepsilon^{3/2} \times f(\varepsilon) d\varepsilon, \quad D_e N = \frac{1}{3} \left(\frac{2e}{m}\right)^{1/2} \int_0^\infty \frac{\varepsilon \times f(\varepsilon) d\varepsilon}{\sum_i \sigma_i^{tr} \times Y_i},$$

$$V_D = -\frac{1}{3} \left(\frac{2e}{m}\right)^{1/2} \left(\frac{E}{N}\right) \cdot \int_0^\infty \frac{\varepsilon}{\sum_i \sigma_i^{tr} \times Y_i} \cdot \frac{df}{d\varepsilon} d\varepsilon, \quad K_{kj} = \left(\frac{2e}{m}\right)^{1/2} \cdot \int_{\varepsilon_{jk}}^\infty \varepsilon \times Q_j^i(\varepsilon) \cdot f(\varepsilon) d\varepsilon.$$

The multiplication of (1) on  $\varepsilon$ ,  $n_e$  and  $N$ , and the integration on  $\varepsilon$  from 0 to  $\infty$  results in the equation of electron energy balance. Left side of (1) gives the power density acquired from electric field:

$$jE = n_e \times e \times V_D \times E = N \times n_e \times e \times V_D \times (E/N). \tag{8}$$

The power density acquired at the collisions with heavy particles having the temperature T is

$$W_H = -n_e \times N \times \sqrt{\frac{2}{m_e}} \times \int_0^\infty \left(kT \times \gamma \times \frac{df}{d\varepsilon}\right) d\varepsilon. \tag{9}$$

The power density lost by electrons at elastic collisions with heavy particles (gas heating) is expressed:

$$W_{el} = n_e \times N \times \sqrt{\frac{2}{m_e}} \times \int_0^\infty \left(2m_e \times \sum_i \frac{Y_i \times \sigma_i^{tr}}{M_i}\right) \times \varepsilon^2 \times f(\varepsilon) d\varepsilon, \tag{10}$$

and on excitation of rotational levels is

$$W_r = n_e \times N \times \sqrt{\frac{2}{m_e}} \times \int_0^\infty 6\varepsilon \times \left(\sum_i B_i \times Y_i \times \sigma_i^r\right) \times f(\varepsilon) d\varepsilon. \tag{11}$$

Every summand in (9–11) gives the input of separate component to appropriate energy loses.

The integration of  $J_{ine}$  gives the difference of power densities lost by electrons at all inelastic collisions of the first kind,  $W_{un}^I$ , and acquired at the collisions of the second kind,  $W_{un}^{II}$ :

$$W_{un}^I - W_{un}^{II} = n_e N \sqrt{\frac{2}{m_e}} \left[ \sum_j \sum_i Y_i \times \varepsilon_{ji} \int_{\varepsilon_{ji}}^\infty \varepsilon \times \sigma_j^i(\varepsilon) \times f(\varepsilon) d\varepsilon - \sum_i \sum_j Y_i \times \varepsilon_{ij} \int_{\varepsilon_{ij}}^\infty \varepsilon \times \sigma_{-j}^i(\varepsilon) \times f(\varepsilon) d\varepsilon \right], \tag{12}$$

where  $y_i \times K_{ji} \times n_e \times N = y_i \times \left[ \sqrt{\frac{2}{m_e}} \int_{\epsilon_{ji}}^{\infty} \epsilon \times \sigma_j^i(\epsilon) \times f(\epsilon) d\epsilon \right] \times n_e \times N$  is the rate of process  $j$ , and impression in a square bracket is rate constant.

The integration of  $J_{ee}$  gives zero.

The relations (8–12) allow calculating the energy fraction inputted to every process,  $\delta$ , as the ratio of power density of appropriate process to total power density. Also, it allows checking the accuracy of EEDF calculations. In our calculation the energy balance was fulfilled with accuracy of  $\sim 0.1\%$ .

The population of vibrational levels of  $N_2$ ,  $O_2$ ,  $H_2O$ , and  $NO$  molecules in ground state was determined by solving the equations system of quasi-stationary kinetics. This system takes into consideration the single-quantum V–V, and V–T exchange between partners, e–V pumping and some other events. The kinetic equation for the concentration,  $[N^{(m)}(V)]$ , molecule of kind  $m$  on the vibrational level  $V$  was written as

$$\begin{aligned} \frac{d[N^{(m)}(V)]}{dt} = & \sum_m \left\{ K_{V-1,V}^{(m)} \times [N^{(m)}(0)] + \sum_{W=0}^{W^*-1} K_{V-1,V}^{(m)W+1,W} \times [N^{(m)}(W+1)] \right\} \times [N^{(m)}(V-1)] \\ & - \sum_m \left\{ (K_{V,V-1}^{(m)} + K_{V,V+1}^{(m)}) \times [N^m(0)] + \sum_{W=1}^{W^*} (K_{V,V+1}^{(m)W,W-1} \times [N^{(m)}(W)]) \right\} \\ & + \sum_{W=0}^{W^*-1} (K_{V,V-1}^{(m)W,W+1} \times [N^{(m)}(W)]) + n_e \times K_{V0}^{(m)} \times [N^m(V)] \\ & + \sum_m \left\{ (K_{V+1,V}^{(m)} \times [N^m(0)]) + \sum_{W=1}^{W^*} (K_{V+1,V}^{(m)W-1,W} \times [N^{(m)}(W-1)]) \right\} \\ & + K_{0V}^{(m)} \times n_e \times [N^{(m)}(0)] \times [N^m(V+1)] + Q_V \end{aligned} \quad (13)$$

where the summation on  $m$  means the summation on amount of components,  $K_{V,V-1}$  and  $K_{V-1,V}$  are the rate constants of V–T exchange,  $K_{V-1,V}^{W+1,W}$  and  $K_{V,V+1}^{W,W-1}$  are the rate constants of V–V exchange,  $K_{V0}$  and  $K_{0V}$  are the rate constants of electron pumping and deactivation of level  $V$ ,  $V$  and  $W$  are the vibrational quantum numbers,  $[N^{(m)}(W)]$  is the concentration of molecule  $m$  on vibrational level  $W$ ,  $Q_V$  is the rates of other reactions,  $W^*$  is the vibrational level corresponding to dissociation limit.  $W^* = 14, 13, 23, 40, 36,$  and  $46$  for  $H_2O(001)$ ,  $H_2O(100)$ ,  $H_2O(010)$ ,  $NO$ ,  $O_2$ , and  $N_2$  molecules, respectively.

Formally, for the molecule with  $W^*$  vibrational levels the systems of  $W^*$  Eqs. (9) for the stationary conditions can be written as:

$$\begin{aligned} a_0 \cdot [N^{(m)}(1)] - b_0 \cdot [N^{(m)}(0)] + d_0 &= 0, \\ a_n \cdot [N^{(m)}(V+1)] - b_n \cdot [N^{(m)}(V)] + c_n \cdot [N^{(m)}(V-1)] + d_n &= 0, \\ -c \times [N^{(m)}(W^*)] - e \times [N^{(m)}(W^*)] + \sum_j Q_j &= 0, \end{aligned}$$

where  $c$ ,  $e$  are the frequencies of dissociation through vibrational continuum for V–V and V–T processes, respectively, the  $\sum_j Q_j$  is the difference of total rates of formation and the losses of vibrational excited molecules for the reactions which are not connected with V–V, V–T exchange and electron excitation-de-excitation,  $n$  is changed from 1 up to  $(W^* - 1)$ .

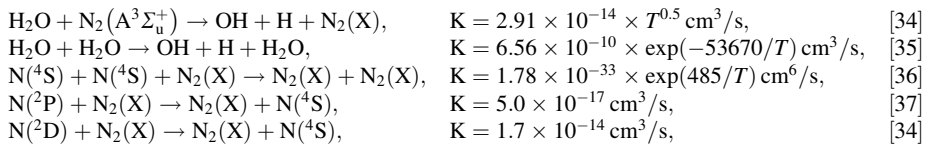
The system is not linear one since its coefficients depend on concentrations. The matrix of system has a three-diagonal form. For this reason we used the same solution method as



for Boltzmann equation. As the zero-order approximation the Boltzmann distribution with vibrational temperature equals to gas one was used. The diagonal prevalence provided the absolute stability of solution. The iterations were terminated when the relative error was <0.001.

The detailed processes list is given in study [13]. The level rate constants were calculated applying SSH (Schwartz–Slawsky–Herzfeld) generalized theory [24]. For normalizing of the rate constants the experimental values of coefficients for  $K_{1,0}$ ,  $K_{0,1}^{1,0}$  of studies [25–30] were used. The molecular parameters were taken from [31, 32] and values of reverse radius in exponential repulsive potential of interaction are given in [33].

The chemical transformations included 187 reactions which describe the concentrations of the following neutral species:  $O_2(X)$ ,  $O_2(a^1\Delta)$ ,  $O_2(b^1\Sigma)$ ,  $O_2(A^3\Sigma)$ ,  $O(^3P)$ ,  $O(^1D)$ ,  $O(^1S)$ ,  $O_3$ ,  $O(3p^3P)$ ,  $O(3s^3S)$ ,  $H_2O$ ,  $H$ ,  $OH$ ,  $H_2O_2$ ,  $HO_2$ ,  $H_2$ ,  $N_2(X)$ ,  $N_2O$ ,  $NO$ ,  $NO_2$ ,  $NO_3$ ,  $HNO$ ,  $HNO_2$ ,  $HNO_3$ ,  $N_2(A^3\Sigma_u^+)$ ,  $N_2(B^3\Pi_g)$ ,  $N_2(C^3\Pi_u)$ , and  $N_2(a^1\Sigma^+)$ . This set was already used by us for the modeling of an atmospheric pressure DC discharge in air [13]. The list of processes and data on the rate constants is given in the same study. We added to this reaction scheme the following reactions:



These reactions were not important for air plasma since in that plasma there were more fast reactions of OH formation and  $N(^4S)$  loss, particularly, the reactions with participation of atomic oxygen.

The modeling was carried out by means of combined solution of all the equations mentioned above for the experimental values of E/N, gas temperature, and discharge current density.

The lack of data on water molecules concentrations is the main problem for the modeling. For this reason, we used these values as fitting parameters to satisfy the measured emission intensities of some  $N_2$  bands and effective vibrational temperatures,  $T_v$ , of  $N_2$  ground state.

The effective vibrational temperature,  $T_v$ , of the  $C^3\Pi_u$  state was obtained using measured intensities,  $I_{V',v''}$ , of  $0 \rightarrow 3$ ,  $1 \rightarrow 4$ ,  $2 \rightarrow 5$ ,  $3 \rightarrow 6$ , and  $4 \rightarrow 7$ ,  $0 \rightarrow 2$ ,  $1 \rightarrow 3$ ,  $2 \rightarrow 4$ ,  $3 \rightarrow 5$ ,  $4 \rightarrow 6$  sequences of bands of the  $C^3\Pi_u \rightarrow B^3\Pi_g$  transition. According to the relation,  $N_{V'} = N_{V'=0} \exp(-\Delta E_{V'}/kT_v)$ , the data obtained were plotted using the coordinates of  $\ln[(A_{0,1}/A_{V',v''})(I_{V',v''}/I_{0,1})] = f(\Delta E_{V'})$ , where  $A_{V',v''}$  is radiation probability of appropriate transition and  $\Delta E_{V'}$  is vibrational energy for  $C^3\Pi_u (V')$  state counted off from  $V' = 0$  level. After fitting the data by using the least-square method, we determined vibrational temperature,  $T_v$ , as the slope of the fitting curve. The linear dependence described the experiment with correlation coefficient greater than 0.99. Both sequences gave the same results. Molecular constants of  $C^3\Pi_u (V')$  state were taken from Ref. [31] and  $A_{V',v''}$  values—from study [37].

For the estimation of population of vibrational levels (vibration temperature) of  $N_2$  ground state, we used two approaches. The first was the direct solution of equation of vibrational kinetics, whereas the second was as follows. We assumed that populations of different  $C^3\Pi_u$  vibration states were reached due to electron impact with the species in vibration levels of  $X^1\Sigma_g^+$  ground states. Also, we assumed that the main process of  $C^3\Pi_u$  vibrational states destruction was not radiation decay but rather quenching via the

collisions with plasma forming gas molecules. Actually, radiation probabilities for different  $C^3\Pi_u$  states are of  $\sim 2 \times 10^7 \text{ s}^{-1}$  [36], whereas quenching rate constants by  $O_2, H_2O$  and  $N_2$  molecules are of  $\sim 10^{-10} \text{ cm}^3/\text{s}$  [38]. At the particle density of  $4 \times 10^{18} \text{ cm}^{-3}$ , the quenching frequency is  $\sim 4 \times 10^8 \text{ s}^{-1}$ . Applying above assumptions, we can write the following five equations since we observed only five transitions from the  $C^3\Pi_u$  ( $V' = 0-4$ ) in irradiation spectra

$$n_e \times N'_{V'=0} \cdot \sum_{V''} [K_{V',0} \exp(-\Delta E_{V'}/kT_{V'})] = Z_Q^{V''=0} \times N''_{V''=0} \times \exp(-\Delta E_{V''=0}/kT_{V''}), \tag{14}$$

$$n_e \times N'_{V'=0} \cdot \sum_{V''} [K_{V',1} \exp(-\Delta E_{V'}/kT_{V'})] = Z_Q^{V''=1} \times N''_{V''=0} \times \exp(-\Delta E_{V''=1}/kT_{V''}), \tag{15}$$

$$n_e \times N'_{V'=0} \cdot \sum_{V''} [K_{V',2} \exp(-\Delta E_{V'}/kT_{V'})] = Z_Q^{V''=2} \times N''_{V''=0} \times \exp(-\Delta E_{V''=2}/kT_{V''}), \tag{16}$$

$$n_e \times N'_{V'=0} \cdot \sum_{V''} [K_{V',3} \exp(-\Delta E_{V'}/kT_{V'})] = Z_Q^{V''=3} \times N''_{V''=0} \times \exp(-\Delta E_{V''=3}/kT_{V''}), \tag{17}$$

$$n_e \times N'_{V'=0} \cdot \sum_{V''} [K_{V',4} \exp(-\Delta E_{V'}/kT_{V'})] = Z_Q^{V''=4} \times N''_{V''=0} \times \exp(-\Delta E_{V''=4}/kT_{V''}), \tag{18}$$

where summation has to include all the vibration levels of the  $X^1\Sigma_g^+$  state;  $N'_{V'} = 0$   $N''_{V''} = 0$  are the  $X^1\Sigma_g^+$  and  $C^3\Pi_u$  concentrations on the zero vibrational level, respectively;  $K_{V',V''}$  is rate constant for excitation of the  $C^3\Pi_u$   $V''$  level from  $X^1\Sigma_g^+$   $V'$  level by electron impact;  $\Delta E_{V'}$ ,  $\Delta E_{V''}$  are vibration energies for the  $X^1\Sigma_g^+$  and  $C^3\Pi_u$  states counted off from zero level, respectively;  $T_{V'}, T_{V''}$  are the “vibrational” temperatures for the  $X^1\Sigma_g^+$  and  $C^3\Pi_u$  states, respectively;  $n_e$  is electron density and  $Z_Q^{V''}$  is quenching frequency. The  $Z_Q^{V''}$  is equal to

$$Z_Q^{V''} = \sum_i (K_{V''}^i \times N^i) + A_{V',V''}$$

where  $K_{V''}^i$  is the quenching rate constant of  $C^3\Pi_u(V'')$  vibrational state by  $O_2, H_2O$  and  $N_2$  molecules,  $N^i$  is the appropriate concentration.

The cross-sections were obtained using the approach described in Ref. [39]. As a result of analyzing different data, it was shown that the cross-sections for  $C^3\Pi_u$  ( $V'$ ) excitation from  $X^1\Sigma_g^+(V'')$  can be written as

$$\sigma_{V',V''}(\varepsilon/\varepsilon(V', V'')) = |M_e|^2 \times q(V', V'') \times F(\varepsilon/\varepsilon(V', V'')),$$

where  $|M_e|^2 = 38 \times 10^{-18} \text{ cm}^2$  is the square of matrix element for electronic transition and  $q(V', V'')$  is the Frank–Condon factor of  $V'-V''$  transition;  $F(\varepsilon/\varepsilon(V', V''))$  is the universal function of the ratio of electron energy to threshold energy.

The system of equations was solved for  $T_{V'}$  by means of Tikhonov’s regularization method [40] using the experimental data on  $T_{V''}$ .

### Results and Discussion

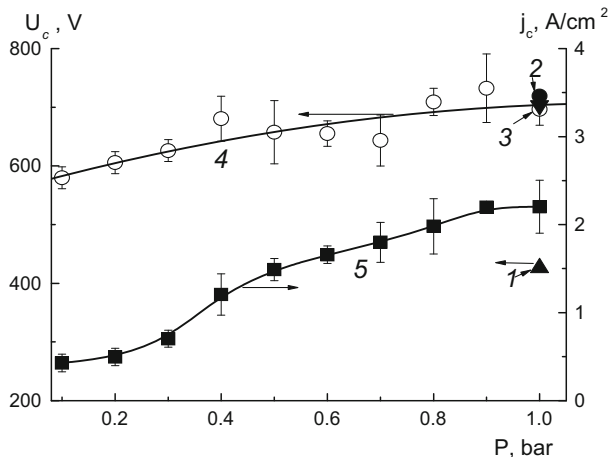
The pressure increase results in a slight growth of cathode voltage drop,  $U_c$ , and in the increase in a cathode current density (Fig. 2). The data on  $U_c$  are close to those obtained in study [5] for atmospheric pressure.

The measured gas temperature (Fig. 3) depends slightly on the pressures in spite of the fact that the specific power ( $j \times E = W$ ,  $j$ —current density) inputted to positive column is increased with the pressure growth from 51 up to  $2.2 \times 10^3$  W/cm<sup>3</sup>. Assuming constant values of  $W$  and heat conductivity coefficient,  $\lambda$ , the solution of heat conductivity equation gives the following expression for the temperature averaged on discharge cross-section,  $\bar{T}$ .

$$\bar{T} = T(R) + 0.125 \times [(W \times \delta) / \lambda] \times R^2, \tag{19}$$

where  $R$ —discharge radius,  $T(R)$ —temperature on the plasma-gas interface,  $\delta$ —energy part transmitting electrons into heat. The pressure growth results in the decrease of  $R$  from 0.21 to 0.072 cm (Fig. 4). The  $(W \times R^2)$  value is increased by a factor of  $\sim 5.1$ . Therefore, the  $\delta$  value has to be decreased with the pressure growth. The EEDF calculations showed that the most part of electron energy is inputted to vibration degree of freedom of N<sub>2</sub> and H<sub>2</sub>O ground states. And this part depends slightly on the pressure. Thus, at the pressure of 1 bar 0.8 of total energy is inputted to N<sub>2</sub>(X,V) and 0.16 to H<sub>2</sub>O (X,V). At the pressure of 0.1 bar 0.81 of total energy is inputted to N<sub>2</sub>(X,V) and 0.11 to H<sub>2</sub>O (X,V). For the direct gas heating over elastic electron collisions with molecules the  $\delta$  is  $\sim 5 \times 10^{-3}$ . Therefore, the main source of gas heating is V-T exchange reactions. If vibrationally excited molecules have no time to relax within discharge zone, it can be expected that the part of vibration energy transforms to heat outside the glowing part of discharge. Actually, the diffusion coefficient,  $D$ , of N<sub>2</sub> in N<sub>2</sub> is equal to  $D = 0.17 \times (T/273)^{1.92}$  at atmospheric pressure [41]. At the discharge of radius,  $R$ , of 0.072 cm (Fig. 4) and at the temperature of 1500 K the diffusion time is equal to  $\tau_D = (R/2.405)^2/D = 4.4 \times 10^{-5}$  s. The characteristic time of V–T relaxation,  $\tau_{VT} = (K_{10} \times [N_2])^{-1}$  is equal to  $1.2 \times 10^{-4}$  s for the same conditions. Therefore, the part of energy which is transformed to heat in the discharge zone can be estimated as  $\tau_D/\tau_{VT} = 0.36$ . It is necessary to point out that for the discharge in argon the all inputted energy is transformed to heat in the glowing part of discharge [12] whereas for air discharge the same behavior of temperature was observed

**Fig. 2** The cathode voltage drop (4) and cathode current density (5) as a pressure function at the discharge current of 40 mA. 1, 2, 3 data for Ar, N<sub>2</sub> and air, respectively from study [5] for the discharge current of 25 mA



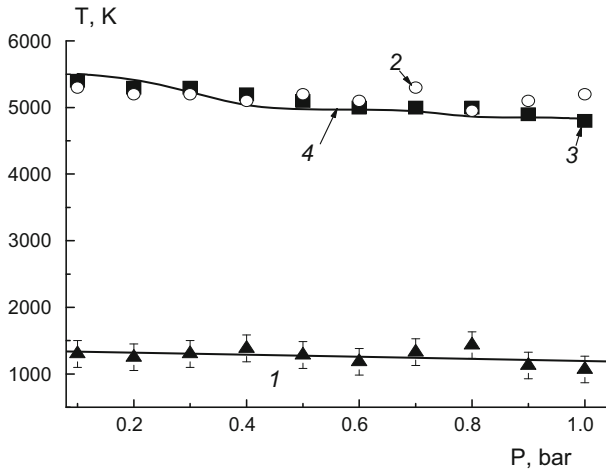
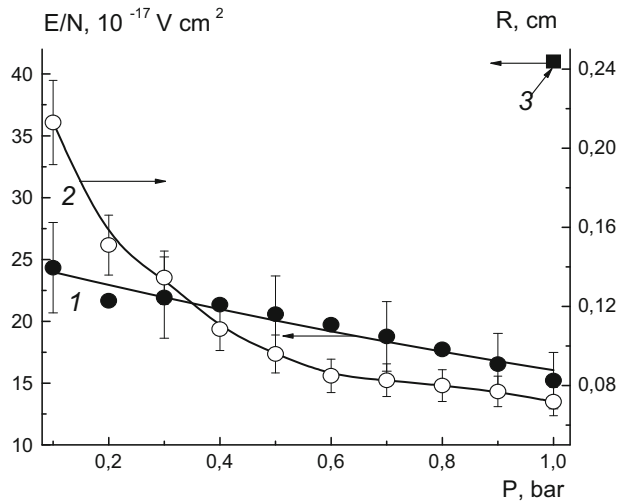


**Fig. 3** The effective vibration (2, 3, 4) and rotational (1) temperatures. 3 were obtained from the solution of Eqs. (1)–(4) for  $N_2$  ground state. 2 are vibration temperatures of  $N_2(C^3\Pi_u)$  state. 4 were obtained from the solution of equations of vibration kinetics for  $N_2$  ground state

**Fig. 4** The reduce electric field strength (1, 3) and radius of positive column (2) as a function of pressure. The discharge current is 40 mA. 3 was calculated by us on data from study [5]



[4]. Moreover, the gas temperatures for both discharges are practically the same. It is no wonder since for both discharges the inputted power is close, most part of energy is inputted to vibrational degree of freedom, and heat conductivity coefficients are close. The similar conclusion on the role of vibrational excited molecules in a gas heating was made in study [42] for DC discharge in air.

Using the measured temperature, we calculated the total concentration of particles ( $P = N \times kT$ ) and values of reduced electric field strengths,  $E/N$ . The appropriate results are shown in Fig. 4. The data on vibrational temperatures for  $C^3\Pi_u$  state are represented in Fig. 3. The gas temperatures,  $E$  and  $E/N$  values for the atmospheric pressure in air [4] and in  $N_2$  were very close.

The OES measurements showed that molecular nitrogen ( $N_2$ ) was represented by bands of second and first positive system ( $C^3\Pi_u \rightarrow B^3\Pi_g, B^3\Pi_g, \rightarrow A^3\Sigma_u^+$ ). Atomic oxygen was represented by lines (777, 845 and 926.6 nm). OH radicals exhibited three bands:  $A^2\Sigma \rightarrow X^2\Pi$  (1–0, 2–1, 3–2). Bands of NO  $\gamma$ -system ( $A^2\Sigma \rightarrow X^2\Pi$ ) were revealed as well. The irradiation of atomic hydrogen was represented by  $H_\alpha$  and  $H_\beta$  lines.

It is difficult to compare correctly the obtained results with data of other studies. An atmospheric pressure DC discharge in  $N_2$  was studied in works [5, 6]. In spite of close values of the most part of external discharge parameters the internal parameters determining a plasma state are essentially differ. Thus, the  $N_2$  rotational temperature measured in study [5] was  $(2900 \pm 200)$  K at atmospheric pressure and current of 25 mA. In study [6] the value of  $(3250 \pm 150)$  K is given for discharge current of 30 mA. The radius of positive column was about 0.6 mm (0.7 mm in our study) [6]. The vibrational temperatures for  $C^3\Pi_u$  state were  $(3500 \pm 200)$  K [5] rather than  $(5000 \pm 200)$  K as in our study (Fig. 3). The bands of  $N_2$  first positive system were not presented in the emission spectrum. At the same time, the values of cathode voltage drop (Fig. 2) and electric field strength in positive column ( $\sim 1$  kV) were practically the same. We assume that such differences are conditioned with the effect of gas flow. The gas residence time in study [5] was 6 min, whereas in our study it was  $\sim 17$  s. Undoubtedly, the increase in gas flow rate can lead to a gas cooling and to water molecules concentration and other neutral species dropping. The passing OH concentration through the maximum under the increase in a gas flow rate was observed in study [43].

The calculations showed that the best agreement between the experimental intensities (Fig. 5), vibrational temperatures (Fig. 3) and the calculation results is achieved at the water content represented in Fig. 6. The calculation was rather sensitive to water content. At experimental values of E/N even several tenths of percent of water influence strongly on EEDF leading to sharp drop of bands intensities. This is due to a large value of momentum transfer cross section of water ( $\sim 10^{-13}$  cm<sup>2</sup>) with respect to appropriate cross section of  $N_2$  ( $\sim 10^{-15}$  cm<sup>2</sup>). Also, the vibrational temperatures were decreased. The calculation shows that the water content at the pressure of 1 bar is  $\sim 1\%$ . At the same time, the water content was estimated in study [6] as 10 % for 30 mA. The water molecules concentration

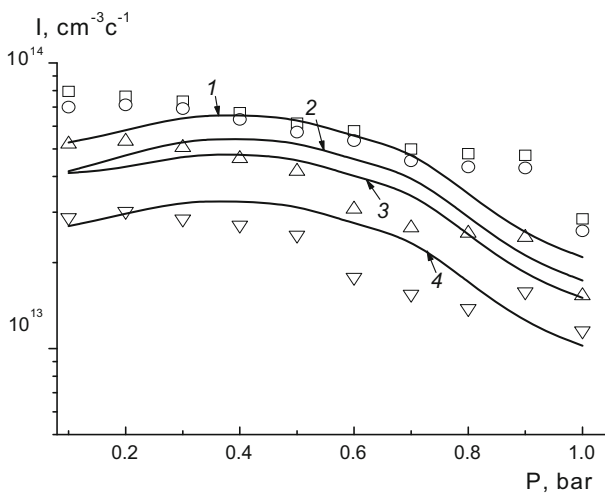
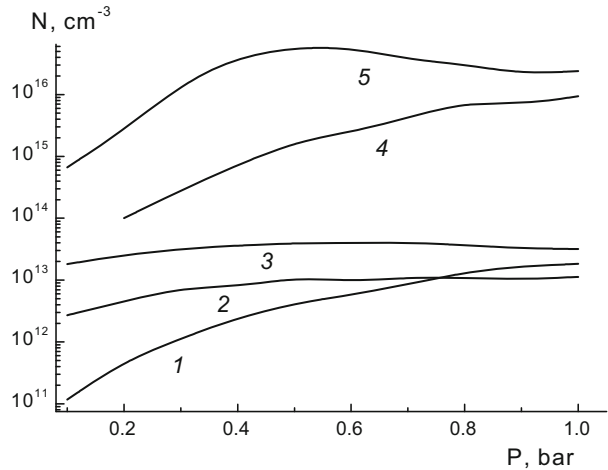


**Fig. 5** Bands intensities of  $N_2$  second positive system ( $C^3\Pi_u \rightarrow B^3\Pi_g$ ). 1, 2, 3, 4  $0 \rightarrow 2, 2 \rightarrow 4, 1 \rightarrow 3, 3 \rightarrow 5$  transitions, respectively. Lines—calculation, points—experiment

**Fig. 6** Concentrations of particles as a function of pressure. 1 NO, 2 O<sub>2</sub>(a<sup>1</sup>Δ<sub>g</sub>), 3 N<sub>2</sub>(A<sup>3</sup>Σ<sub>u</sub><sup>+</sup>), 4 HNO, 5 H<sub>2</sub>O



depends on the balance of water rate evaporation and its pumping. We can suppose that the evaporation rate in the given study and in study [6] must be close, since the cathode current density and the cathode voltage drop are the same. Probably, faster pumping in our case provides lower density of water molecules in the discharge. Therefore, it can be expected that the concentrations of species formed from water have to be lower than in studies [5, 6].

The results of calculations of main discharge species are shown in Figs. 6, 7. The main species forming in a discharge were OH, H<sub>2</sub>O<sub>2</sub>, NO, and N<sub>2</sub>(A<sup>3</sup>Σ<sub>u</sub><sup>+</sup>) molecules. For the same discharge current the concentrations of these species in air were essentially more [13]. Thus, OH, H<sub>2</sub>O<sub>2</sub>, NO concentrations for N<sub>2</sub> discharge were  $\sim 1 \times 10^{14}$ ,  $8.9 \times 10^{12}$ , and  $1.8 \times 10^{12} \text{ cm}^{-3}$ , respectively, whereas for air discharge  $3 \times 10^{14}$ ,  $2.7 \times 10^{14}$ , and  $7 \times 10^{16} \text{ cm}^{-3}$ , respectively. This fact is conditioned not only difference in O<sub>2</sub> content but the different EEDF. In air discharge the EEDF is “richer” with fast electrons. And rate coefficients of electron impact are more. The electron average energy for air discharge is 1.1 eV whereas for N<sub>2</sub> one is 0.96 eV.

In fact, at atmospheric pressure the OH density was  $\sim 1 \times 10^{14} \text{ cm}^{-3}$ , whereas the value of  $2 \times 10^{15} \text{ cm}^{-3}$  was obtained in study [6]. To understand the difference, we carried out the calculations using experimental results of [5, 6] as input data for our model. These data were the following:  $E - 1 \text{ kV}$ , gas temperature—3000, discharge current—30 mA, discharge radius—0.6 mm, gas temperature—3000 K, water molecules content—10 %, pressure—1 bar. It gives the  $E/N$  of  $4.1 \times 10^{-16} \text{ V} \times \text{cm}^2$ . The calculation gives the values close to experimental data: OH concentration— $1.1 \times 10^{15} \text{ cm}^{-3}$ , vibrational temperature of N<sub>2</sub>(X)—3100 K. The higher temperature in [5, 6] results in the lower ( $\sim 2$  times) concentration of plasma-forming gas molecules and in the higher  $E/N$  value ( $1.6 \times 10^{-16} \text{ V} \times \text{cm}^2$  in our experiment). It leads to the electron drift velocity increase and higher values of rate coefficients of electron impact. The increase degree depended on the process threshold energy. Thus, the rate constant for excitation of N<sub>2</sub>(X,  $V = 1$ ) was increased by a factor of 2 only, whereas the rate constant of N<sub>2</sub>(A<sup>3</sup>Σ<sub>u</sub><sup>+</sup>) excitation was increased by a factor of  $\sim 10^2$ . Due to the increase in drift velocity the electron density was decreased by a factor of  $\sim 2$  in comparison with our data represented in Fig. 8. The average electron energy was 1.22 eV (0.96 eV in our study, Fig. 8) and electron density was  $3.1 \times 10^{12} \text{ cm}^{-3}$  ( $7 \times 10^{12} \text{ cm}^{-3}$  in our study). Estimations made in study [6] give

**Fig. 7** Concentrations of particles as a function of pressure. 1 HO<sub>2</sub>, 2 H<sub>2</sub>O<sub>2</sub>, 3 H<sub>2</sub>, 4 OH

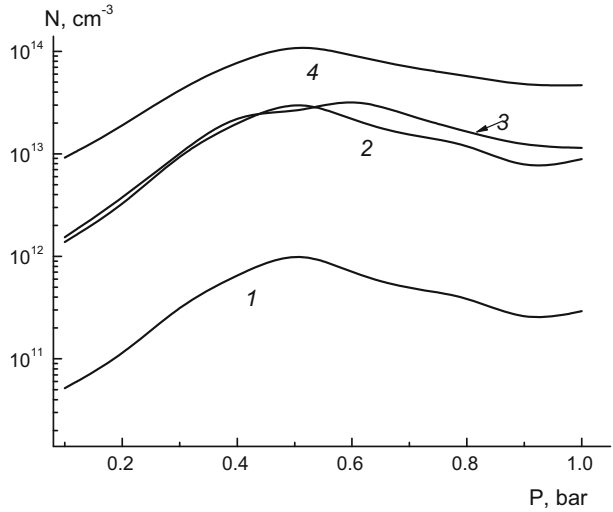
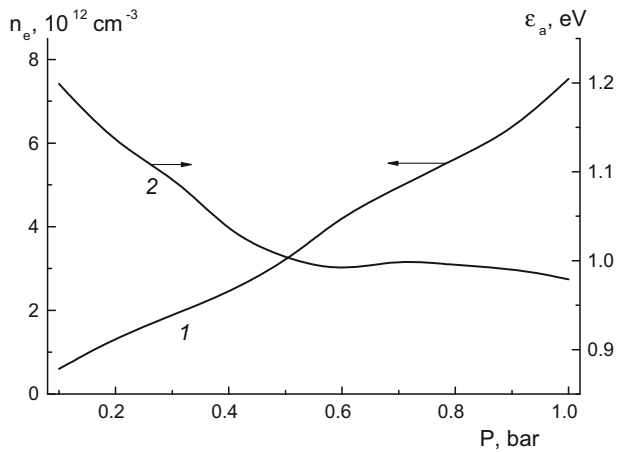
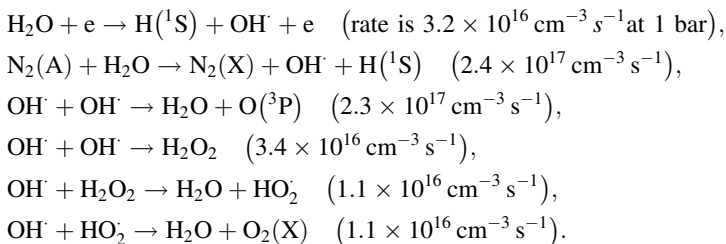


**Fig. 8** The electron density (1) and average electron energy (2) as a pressure function



the close value of  $T_e \approx 1 \text{ eV}$ , but electron density was essentially more  $(2\text{--}6) \times 10^{14} \text{ cm}^{-3}$ . As the result of action of factors mentioned above, the rates of main processes of water dissociation were increased essentially (see below). Calculations show that the following reactions are the main ones for the water dissociation and OH losses at any pressures:



At the conditions of study [5, 6] the dissociation rates by electron impact and via  $N_2(A)$  collisions were  $8.8 \times 10^{18}$  and  $8.6 \times 10^{19} \text{ cm}^{-3} \text{ s}^{-1}$ , respectively. In spite of high value of temperature the rate of thermal dissociation was negligible ( $6.6 \times 10^{17} \text{ cm}^{-3} \text{ s}^{-1}$ ).

The difference in vibrational temperatures is conditioned with the following reasons. The excitation frequencies of vibrational levels with the electron impact change slightly. But higher temperatures result in the increase in both the rate constants of V–T and V–V exchange. However, V–T rate constants are increased essentially more than V–V ones. According to [24] the V–V rate constant is  $K_{10}^{01} = 4.54 \cdot 10^{-10} \exp(-23.99 \times T^{-0.14})$  and V–T rate constant is  $K_{10} = 4.15 \times 10^{-29} \exp(2.303 \times T^{0.357})$ . It gives  $K_{10} = 1.7 \times 10^{-15} \text{ cm}^{-3} \text{ s}^{-1}$  at 1500 K and  $K_{10} = 1.1 \times 10^{-11} \text{ cm}^{-3} \text{ s}^{-1}$  at 3000 K. For the  $K_{10}^{01}$  values, we obtain  $8.2 \times 10^{-14}$  and  $1.8 \times 10^{-13} \text{ cm}^{-3} \text{ s}^{-1}$  for the same temperature. The predominance of V–T exchange over V–V one leads to equalizing the gas temperature and the vibrational one. Vibrational degrees of freedoms are practically in equilibrium with translation ones.

The results of vibrational distributions calculations are shown in Fig. 9. It is clearly seen that the distributions are not equilibrium ones. But for lower levels, distributions can be approximated by Boltzmann's equation. Therefore, the suppositions, which were used for the derivation of Eqs. (14)–(18) are valid. The sharp bend at  $V = 12$  reflects the action of the reaction  $N_2(X, V > 12) + O(^3P) \rightarrow NO + N$  [44]. At low  $V$  values the V–V exchange is predominant. It provides the decrease in population of vibrational levels with  $V$  increase. But V–T rate constants rise with  $V$  faster than V–V ones. And at  $V > 12$  the V–T processes start to dominate forming the characteristic “lplateau”. It is necessary to point out that the data on vibrational temperatures obtained by two different methods (from the solution of vibrational kinetic equations and from the bands intensities using Eqs. (1)–(5) agree quite well. And the vibrational temperatures of  $N_2$  ( $C^3\Pi_u$ ) state can be used for estimation of vibrational temperatures of  $N_2$  ground state. Such simple measurements of bands intensities will allow taking into account the second kind collisions of electrons with  $N_2(X)$  vibrational excited molecules at EEDF calculations. Our data represented in Fig. 10

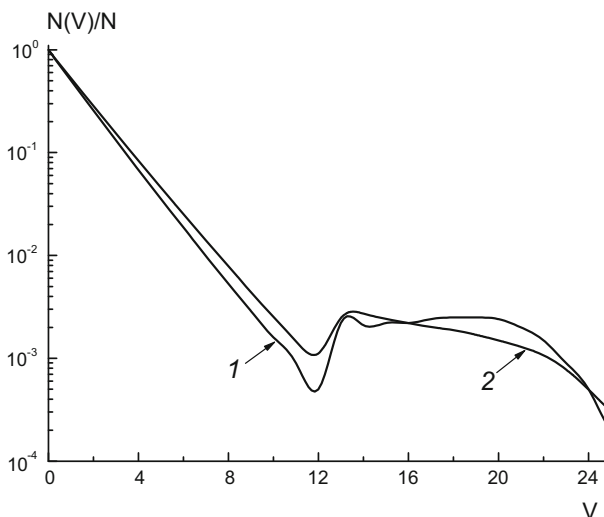
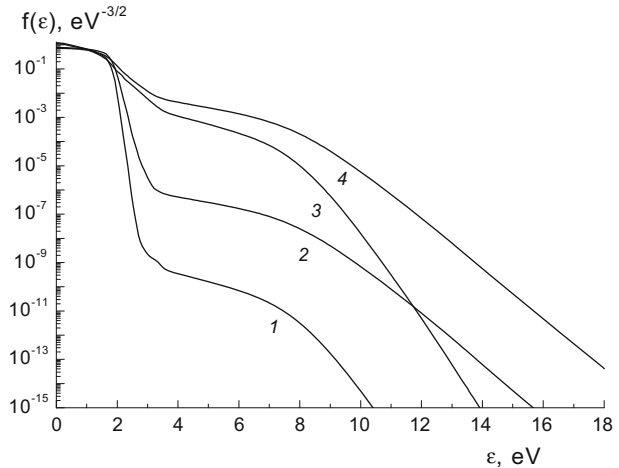


**Fig. 9** The normalized distribution of  $N_2(X)$  molecules on vibration levels, / 1 bar; 2 0.1 bar



**Fig. 10** Calculated EEDF. 1, 3 at the pressure of 1 bar. 2, 4 at the pressure of 0.1 bar. 1, 2 second kind collisions with vibration excited  $N_2(X)$  did not take into account. 3, 4 second kind collisions with vibration excited  $N_2(X)$  were taken into account



show that it is necessary to do. The super-elastic collisions influence very strongly the high energy part of EEDF and, as the result, the rate constants of electron excitation processes with the high threshold energies.

The  $N_2$  vibrational temperatures obtained in [4, 13] for air plasma of atmospheric pressure were 1000 K less than in given study. Calculations showed that the temperature decrease is not connected with the presence of  $O_2$  molecules because the rate constants of V–T exchange for  $N_2$ – $N_2$  and  $N_2$ – $O_2$  collisions are close. The main reason is the decrease in the excitation frequency by electron impact due to the difference in electron drift velocities. For  $N_2$  discharge the electron density was  $7.6 \times 10^{12} \text{ cm}^{-3}$  whereas for air discharge— $2.5 \times 10^{12} \text{ cm}^{-3}$ .

The calculation was very sensitive to water content. The increase in water mole fraction leads to the decrease in calculated band intensities and to the dropping effective vibrational temperatures of  $N_2(X)$ . The momentum transfer cross-section for  $H_2O$  is higher than for  $N_2$  by a two order of magnitude. It provides the decrease in the EEDF “tail” and, as the result, in the essential dropping rate constants of electron impact processes with the high threshold energy. Such influence of water content on electron kinetic parameters is not specific feature of  $N_2$  plasma. The same situation takes place for oxygen plasma as well [45]. The vibrational quantum of  $N_2(X)$ ,  $2359 \text{ cm}^{-1}$ , is less than for  $H_2O$  (010) mode ( $1595 \text{ cm}^{-1}$ ). The rate constant of  $N_2$  V–T exchange on  $H_2O$  is higher than for  $N_2$ – $N_2$  exchange by a factor of 34 at 1500 K. The rate constant for V–V process  $N_2(X, V = 1) + H_2O(000) \rightarrow N_2(X, V = 0) + H_2O(010)$  is higher than for  $N_2(X, V = 1) + N_2(X, V = 0) \rightarrow N_2(X, V = 0) + (X, V = 1)$  by a factor of 25. It gives the decrease in the population of  $N_2(X)$  vibrational levels under water molecule content growth. In turn, this decrease leads to the decrease in the EEDF “tail” over the collisions of the second kind.

## Conclusion

In the present study, the DC discharge in  $N_2$  was examined in a pressure range of 0.1–1 bar at the discharge current of 40 mA. The changes in the gas temperatures, electric field strengths, cathode voltage drop, intensities of some  $N_2$  bands, and vibrational temperatures

of  $N_2(C^3\Pi_u)$  were measured. On the base of these data, the model of discharge was developed. The model included the joint solution of Boltzmann equation, equations of vibrational kinetics and equations of chemical kinetics. Calculations on that model agree with the measured bands intensities and vibrational temperatures. In addition, the proposed model explains the results of other studies. The  $N_2(X)$  vibrational molecules were shown to influence strongly the EEDF over the super elastic collision. The main species of plasma were  $H_2O$ ,  $OH$ ,  $H_2O_2$ ,  $O(^3P)$  and  $HO_2$ .

**Acknowledgments** This study was supported by the RFBR grant, project number 14-02-01113 A.

## References

1. Bruggeman P, Leys C (2009) *J Phys D Appl Phys* 42(5):053001
2. Tatarova E, Bundaleska N, Sarrette J, Ferreira CM (2014) *Plasma Sources Sci Technol* 23(6):063002
3. Jiang B, Zheng J, Qiu S, Wu M, Zhang Q, Yan Z, Xue Q (2014) *Chem Eng J* 236:348–368
4. Titov VA, Rybkin VV, Maximov AI, Choi H-S (2005) *Plasma Chem Plasma Process* 25(5):502–518
5. Verreycken T, Schram DC, Leys C, Bruggeman P (2010) *Plasma Sources Sci Technol* 19(4):045004
6. Li L, Nikiforov A, Xiong Q, Lu X, Taghizadeh L, Leys C (2012) *J Phys D Appl Phys* 45(12):125201
7. Nikiforov A, Li L, Xiong Q, Leys C, Lu XP (2011) *Eur Phys J Appl Phys* 56(2):24009
8. Ito H, Kano H (2008) *Appl Phys Express* 1:10601–10603
9. Liu DX, Bruggeman P, Iza F, Rong MZ, Kong MC (2010) *Plasma Sources Sci Technol* 19(2):025018
10. Zhang S, Van Gaens W, Van Gessel B, Hofman S, Van Veldhuizen E, Bogaerts A, Bruggeman P (2013) *J Phys D Appl Phys* 46(20):205202
11. Van Gaens W, Bruggeman PJ, Bogaerts A (2014) *New J Phys* 16:063054
12. Shutov DA, Smirnov SA, Bobkova ES, Rybkin VV (2014) *Plasma Chem. DOI, Plasma Process.* doi:10.1007/s11090-014-9596-3
13. Bobkova ES, Smirnov SA, Zalipaeva YV, Rybkin VV (2014) *Plasma Chem Plasma Process* 34(4):721–743
14. Bruggeman P, Schram D, Gonzalez MA, Rego R, Kong MG, Leys C (2009) *Plasma Sources Sci Technol* 18(2):025017
15. Titov VA, Rybkin VV, Smirnov SA, Kulentsan AN, Choi H-S (2006) *Plasma Chem Plasma Process* 26(6):543–555
16. Raizer YuP (1991) *Gas discharge physics*. Springer, Berlin
17. Gordiets BF, Ferreira CM, Guerra VL, Loureiro J, Nahorny J, Pagnon D, Touzeau Vialle M (1995) *IEEE Trans Plasma Sci* 23(23):750–768
18. Kajita S, Ushiroda S, Kondo Y (1990) *J Phys D Appl Phys* 67(9):4015–4023
19. Rybkin VV, Titov VA, Kholodkov IV (2008) *Izv Vyssh Uchebn Zaved Khim Khim Tekhnol* 51(3):3–10 (in Russian)
20. Rybkin VV, Titov VA, Kholodkov IV (2009) *Izv Vyssh Uchebn Zaved Khim Khim Tekhnol* 52(12):3–10 (in Russian)
21. Laher RR, Gilmore FR (1990) *J Phys Chem Ref Data* 19(1):277–304
22. Loureiro J, Ferreira CM (1989) *J Phys D Appl Phys* 22(11):1680–1691
23. Diamy A-M, Legrand J-C, Smirnov SA, Rybkin VV (2005) *Contrib Plasma Phys* 45(1):5–21
24. Schwartz RN, Slawsky ZI, Herzfeld KF (1952) *J Chem Phys* 20(10):1591
25. Capitelli M (ed) (1986) *Nonequilibrium vibrational kinetics*. Springer, Berlin
26. Kiefer JH (1972) *J Chem Phys* 57(5):938–1956
27. Mnatsakanyan AK, Naidis GV (1985) *High Temperature (Teplofizika Vysokikh Temperatur)* 23(4):640–646 (in Russian)
28. Salnikov VA, Starik AM (1995) *High Temperature (Teplofizika Vysokikh Temperatur)* 33(1):121–133 (in Russian)
29. Wysong IJ (1994) *J Chem Phys* 101(4):2800–2810
30. Frost MJ, Islam M, Smith IWM (1994) *Can J Chem* 72(3):606–611
31. Huber KP, Herzberg G (1979) *Molecular spectra and molecular structure IV. Constants of diatomic molecules*. Litton Educational Publishing, Inc, New York
32. Glushko VP (ed) (1978) *Thermodynamic properties of individual substances. Handbook*. Nauka, Moscow (in Russian)

33. Radtsig AA, Smirnov BM (1980) Handbook on atomic and molecular physics. Atomizdat, Moscow (in Russian)
34. Herron JT (1999) *J Phys Chem Ref Data* 28(5):1453–1483
35. Javoy S, Naudet V, Abid S, Paillard CE (2003) *Exp Thermal Fluid Sci* 27(4):371–377
36. Clyne MAA, Stedman DH (1967) *J Phys Chem* 71(9):3071–3073
37. Nicholls RW (1964) *Ann Geophys* 20:144–151
38. Pancheshnyi SV, Starikovskaia SM, Starikovskii AY (1998) *Chem Phys Lett* 294(6):523–527
39. Slovetskiy DI (1980) Mechanism of chemical reactions in the non-equilibrium plasma. Nauka, Moscow (in Russian)
40. Tikhonov AN, Arsenin VY (1974) Methods of solution of incorrect tasks. Nauka, Moscow (in Russian)
41. Grigoriev IS, Meilylikhov EZ (eds) (1991) Physical quantities. Handbook. Energoatomizdat, Moscow (in Russian)
42. Staack D, Farouk B, Gutsol A, Fridman A (2005) *Plasma Sources Sci Technol* 14(4):700–711
43. Kim YH, Hong YJ, Baik KY, Kwon GC, Vhoi JJ, Cho GS, Uhm HS, Kim DY, Choi EH (2014) *Plasma Chem Plasma Process* 34(3):457–472
44. Smirnov SA, Rybkin VV, Kholodkov IV, Titov VA (2002) *High Temp* 40(3):323–330
45. Bobkova ES, Rybkin VV (2013) *High Temp* 51(6):747–752